LAWRENCE
LIVERMORE
NATIONAL
LABORATORY

LLNL-JRNL-736176

Cement as a container for nuclear fission products: the case of 90Sr and its daughters

L. Dezerald, J. Kohanoff, A. A. Correa, A. Caro, R. Pellenq, F. Ulm, A. Saul

August 3, 2017

Environmental Science and Technology

Disclaimer

This document was prepared as an account of work sponsored by an agency of the United States government. Neither the United States government nor Lawrence Livermore National Security, LLC, nor any of their employees makes any warranty, expressed or implied, or assumes any legal liability or responsibility for the accuracy, completeness, or usefulness of any information, apparatus, product, or process disclosed, or represents that its use would not infringe privately owned rights. Reference herein to any specific commercial product, process, or service by trade name, trademark, manufacturer, or otherwise does not necessarily constitute or imply its endorsement, recommendation, or favoring by the United States government or Lawrence Livermore National Security, LLC. The views and opinions of authors expressed herein do not necessarily state or reflect those of the United States government or Lawrence Livermore National Security, LLC, and shall not be used for advertising or product endorsement purposes.

LLNL-JRNL-736176

Cement as a container for nuclear fission products: the case of ^{90}Sr and its daughters

L. Dezerald,[1,2] J. Kohanoff,[3] A. A. Correa,[4] J. Caro,[5] R. Pellenq,[1,2,6] F. Ulm,[1,2] and A. Saúl[1,2,6,*]

[1] *Department of Civil and Environmental Engineering, Massachusetts Institute of Technology,*
[2] *MultiScale Material Science for Energy and Environment, UMI 3466 CNRS-MIT, 77 Massachusetts Avenue, Cambridge CA 02139, USA*
[3] *Atomistic Simulation Centre, Queen's University Belfast, Belfast BT7 1NN, United Kingdom*
[4] *Condensed Matter and Materials Division, Physical and Life Sciences Directorate, Lawrence Livermore National Laboratory, Livermore, California 94550, USA*
[5] *Los Alamos National Laboratory, Los Alamos New Mexico 87545, USA*
[6] *Aix-Marseille University, CINaM-CNRS UMR 7325 Campus de Luminy, 13288 Marseille cedex 9, France*

(Dated: May 21, 2015)

One of the main challenges faced by the nuclear industry is the long-term confinement of nuclear waste. Because it is inexpensive and easy to manufacture, cement is the material of choice to store large volumes of radioactive materials, in particular the low-level medium-lived fission products. It is therefore of utmost importance to assess the chemical and structural stability of cement containing radioactive species. Here, we use *ab-initio* calculations based on density functional theory (DFT) to study the effects of ^{90}Sr insertion and decay in C-S-H (calcium-silicate-hydrate) in order to test the ability of cement to trap and hold this radioactive fission product and to investigate the consequences of its β-decay on the cement paste structure. We show that ^{90}Sr is stable when it substitutes the Ca^{2+} ions in C-S-H, and so is its daughter nucleus ^{90}Y after β-decay. This suggests that cement could be used for ^{90}Sr storage. Interestingly, ^{90}Zr, daughter of ^{90}Y and final product in the decay sequence, is found to be unstable in these sites.

I. INTRODUCTION

Long-term confinement of radioelements produced by nuclear fission is one of the main challenges faced by the nuclear industry. The primary focus of the nuclear waste storage research has long been oriented towards host materials that can handle the large structural damage induced by the high-energy α-decay of actinides.[1,2] However, the need for optimising the vitrification process of actinides[1] and for increasing the capacity of repositories[3] has prompted the investigation of other forms of containers specifically targeted at low- and medium-level waste. Such containers became urgently needed after the Fukushima disaster, where large volumes of contaminated soils, water and buildings had to be quickly handled.[4–7] The main concern lies in the management of the medium-lived β^--emitter fission products, ^{137}Cs and ^{90}Sr.[4,5] These represent the largest fraction of the nuclear waste volume,[8] and have been found in the surrounding areas and in the cooling water of the damaged power plants.[4,5] They present important health risks: ^{137}Cs β^- decay is followed by a hazardous γ emission, while ^{90}Sr can contaminate the animal and human population due to its ability to replace the isovalent Ca ions that constitute bones and teeth (hence the name *bone seeker*). This is particularly dangerous as β-emission in the bone produces a low-energy electron cascade that can reach stem cells in the bone marrow, this being a major cause of leukaemia.

β^- decay produces modifications of the host matrix chemistry and can also influence its mechanical properties. The three main processes following β-decay are: (1) the emission of the β electron at MeV energies, (2) the recoil of the transmuted nucleus with kinetic energies in the eV range due to conservation of momentum, and (3) the electronic rearrangement around the transmuted nucleus due to the sudden increase in nuclear charge ($Z \rightarrow Z+1$). All of these processes interact with the host in different ways.[1,9–11] Recent theoretical studies of the effects of transmutation due to β^- decay of ^{137}Cs and ^{90}Sr in ceramics and oxides[12] showed important chemical and structural modifications of the host material in the case of radioparagenesis[11,13] in which a solid-state daughter phase is derived radiogenically by a parent phase. These studies enable the design of wasteforms with improved mechanical properties by means of transmutation, thus opening a promising avenue for long-term nuclear waste containment. A different, although related matter is the assessment of the ageing of materials partially contaminated by hosting nuclear waste, which is the main focus of the present work.

Here we investigate the local effects of ^{90}Sr contamination and transmutation on cement. ^{90}Sr (half-life 28.79 years) undergoes two successive β^- decays to ^{90}Y (half-life 64 hours), and to ^{90}Zr (stable). Compared to specifically designed glass or ceramic nuclear waste containers, cement is inexpensive, easy to manufacture, easy to formulate by mixing with other materials such as blast furnace slag,[14] and it benefits from centuries of use and decades of research related to the civil engineering industry. This makes cement the primary candidate for large volumes of low-level nuclear waste storage in post-accidental conditions. So far, most of the research on irradiated cement has focused on its ability to capture radioelements, and on their leaching from cement containers.[8,15–21] As mentioned above, ^{90}Sr capture in cement is very likely because of Ca-Sr isovalence, Ca being present in C-S-H (calcium-silicate-hydrate), which is

the principal binding product of cement hydration.[22–24] Although recent atomistic simulations showed that ^{90}Sr capture by C-S-H does not modify the elastic properties of cement,[25] the consequences of ^{90}Sr transmutation via β^- decay on C-S-H structure and chemical properties are still largely unknown.

In this work we investigate the consequences of ^{90}Sr transmutation in C-S-H using calculations based on Density Functional Theory (DFT), which is an appropriate tool to account for the electronic and chemical properties of the cement paste as well as those of the investigated radionuclides. The chemical and physical mechanisms at stake in ^{90}Sr capture were investigated by substituting Ca^{2+} ions in the atomistic model of C-S-H proposed in References [26], [27], and [28]. ^{90}Sr was then successively replaced by its daughter nucleus, ^{90}Y and ^{90}Zr, to study the stability of these elements in cement paste. DFT molecular dynamics (DFMD) simulations were then performed to investigate the possible chemical and structural modifications induced locally in C-S-H contaminated by ^{90}Sr and its successive transmutations.

In Sec. II we present the atomistic model and summarize the details of the calculation method. The results of the substitution energies of Ca by ^{90}Sr, ^{90}Y, and ^{90}Zr in C-S-H are presented in Sec. III A and the corresponding effects of temperature in Sec. III B. A general discussion of the results by an analysis of the pair distribution function and the Bader analysis of the charges is exposed in Sec. IV. Finally, we present conclusions and a summary in Sec. V.

II. METHODOLOGY

C-S-H, the principal binding phase responsible of the strength of cementitious materials, precipitates as nanoscale clusters when mixing water with di-calcium (C_2S) and tri-calcium silicate (C_3S). Given its complex structure and composition, the atomic structure of C-S-H has traditionally been based on Taylor's postulate that C-S-H is a structurally imperfect layered hybrid of two natural minerals,[29] tobermorite of 14 Å interlayer spacing[30] and jennite.[31] These minerals reproduce the laminar structure of C-S-H where calcium ions are located between layers of silicate chains. However, limitations of these models emerged when it became possible to further characterize experimentally the C-S-H molecular composition, notably the average calcium to silicon ratio (C/S = 1.7) and the density of the C-S-H particle (2.6 g/cm^3).[32–35] These values cannot be obtained from either tobermorite 14 Å (C/S = 0.83 and 2.18 g/cm^3) or jennite (C/S = 1.5 and 2.27 g/cm^3).

The atomic structure for C-S-H used in this work has recently been proposed in order to bridge the gap between atomic-scale simulations and experiments.[26–28] It is presented in Fig. 1 and was generated following the procedure reported in Ref. [26]. The cell contains 501 atoms and has the chemical composition $Ca_{72}Si_{44}O_{235}H_{150}$, with a C/S ratio of 1.65 and a density of 2.56 g/cm^3 in very good agreement with experimental data.[32–35] Figure 1 shows the silicate chains formed by corner sharing SiO_4^{4-} tetrahedra. These chains, which form the characteristic layered structure of C-S-H, have been randomly broken to obtain the desired C/S ratio[26–28]. It can also be seen that the Ca^{2+} ions appear in two distinct environments: intralayer and interlayer. Water, in the form of H_2O molecules and OH^- groups, is present in the interlayer space.

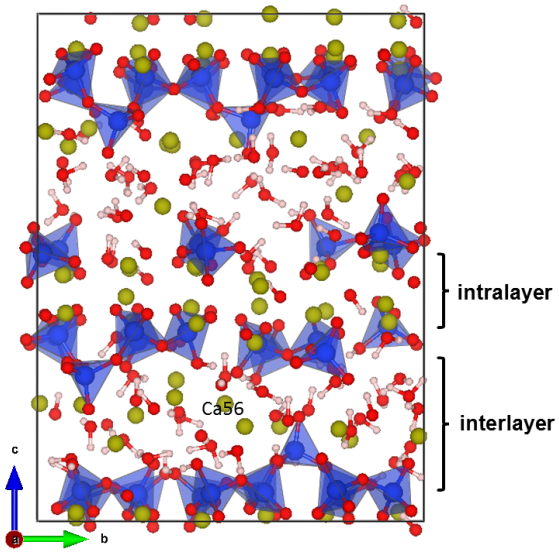

FIG. 1. (color online) Schematic representation of the C-S-H structure. Hydrogen atoms are in white, oxygen atoms in red, calcium in yellow, and Si in blue. The corner sharing SiO_4^{4-} tetrahedra forming the silicate chains are also shown.

First-principles electronic structure calculations were performed within the DFT framework using the Quantum-espresso plane-wave code.[36] We used the Perdew-Burke-Ernzerhof generalized gradient approximation (PBE-GGA)[37] and ultrasoft pseudopotentials with explicit semi-core electrons. The plane-wave cutoff for the Kohn-Sham orbitals was set to 80 Ry and all the calculations were performed at constant volume with a single **k**-point (the Γ-point). Residual forces on the atoms after geometric relaxation were smaller than 10^{-2} eV/Å.

We first performed a 1.2 ps DFMD simulation at 300 K to check the local stability of the C-S-H structure used. We then performed a set of DFMD simulations to study possible displacements of the substitute radioelements in the cement matrix. Given the computational load of DFMD calculations, the latter were performed for only one of the 72 Ca sites (site number 56, interlayer, indicated in Fig. 1). These simulations were aimed at verifying that the preferred site for the substituting atoms corresponded to the site previously occupied by the Ca ion. When this was not the case, the simulations allowed us to investigate the structural modifications induced by

^{90}Sr insertion and decay in C-S-H.

III. RESULTS

A. Substitution and decay of ^{90}Sr in Ca sites

C-S-H contamination was investigated by substituting one by one each Ca ion by Sr. The chemical effects of ^{90}Sr transmutation via β^- decay in C-S-H were then studied by substituting Ca with Y and Zr, successively. The C-S-H cell after substitution, denoted $Ca_{n-1}X$ where X stands for Sr, Y or Zr, has the chemical composition $Ca_{71}XSi_{44}O_{235}H_{150}$. Each substitution is followed by relaxation of the atomic positions. The substitution energy $\Delta E_X(i)$ is defined as:

$$\Delta E_X(i) = E_{Ca_{n-1}X}(i) - E_{Ca_n} + E_X^{bulk} - E_{Ca}^{bulk} \quad (1)$$

where $E_{Ca_{n-1}X}(i)$ is the energy of the cell containing element X at site i, E_{Ca_n} is the energy of C-S-H before substitution, and E_X^{bulk} are the energies of the bulk phases: face-centered cubic for Ca and Sr, and hexagonal close-packed for Y and Zr. The calculated substitution energies for Sr, Y and Zr in each one of the 72 Ca sites of the simulation cell are presented in Fig. 2.

Figure 2(a) shows the results for Sr. As expected from the isovalence between Sr and Ca, the substitution energy is generally low (0.15 eV on average), with 7 negative values. Negative ΔE_{Sr} values indicate sites where Sr is more stable than Ca, and will tend to substitute it, thus contaminating the sample. To further analyze the data, we divided Fig. 2(a) into two sections marked by a vertical line: the first 48 sites correspond to intralayer Ca sites trapped between silicate chains, and the remaining 24 sites (number 49 to 72) correspond to the interlayer area, where the Ca ions co-exists with water molecules and OH^- groups. We also show in Fig. 2(a) the average substitution energy calculated separately for the intra and interlayer with a horizontal blue line; the substitution energies for ^{90}Sr are, on average, lower in the interlayer (0.08 eV) than in the intralayer (0.19 eV). It is interesting to note here that due to the configurational entropy contribution to the free energy, solution energies of this order of magnitude imply quite a large solubility limit even at room temperature. A regular solution model with a solution energy of 0.08 eV gives, for example, a solubility at room temperature of 4%, thus suggesting that cement in contact with Sr-contaminated water will naturally incorporate this amount of Sr.

In order to investigate the chemical effects of ^{90}Sr β^- decay on C-S-H structure, we calculated the substitution energy of Y in all 72 Ca sites. The results are presented in Fig. 2(b), and the calculated average substitution energies are gathered in Table I. Fig. 2(b) shows that the substitution energy of Y is generally lower than that of Sr, with a larger dispersion and an average value of 0.05 eV. Overall, 28 sites substituted with Y display a negative ΔE_Y. Y is consequently more stable in C-S-H than Sr, which is surprising because, with a theoretical charge of +3, Y is not isovalent with Ca. The average substitution energy is lower but still positive in the intralayer region (0.11 eV), and it is now negative in the interlayer spacing (-0.09 eV). We also notice that the difference between the average substitution energy in the intra and interlayer regions is larger for ^{90}Y (0.20 eV) than for ^{90}Sr (0.11 eV).

The substitution energies of ^{90}Zr, daughter nucleus of ^{90}Y also through β^- decay, are given for the 72 sites in Fig. 2(c). Contrary to Sr and Y, the calculated energies are all positive, large and widely dispersed around the average value of 2.34 eV, which is more than one order of magnitude larger than that of Sr. Fig. 2(c) shows again an enhanced stability upon substitution in the interlayer relative to the intralayer region, while the energy difference between intra and interlayer substitution is the largest (0.45 eV).

Finally, we have also verified that Sr in C-S-H prefers to substitute Ca rather than Si (present in the silicate chains). Substitution energies obtained for Sr replacing Si are around 4 eV, which are 10 times larger than those obtained when Sr replaces Ca, thus rendering this process extremely unlikely. This is expected from the charge unbalance locally originated by such a substitution.

B. Effects of temperature on contaminated C-S-H

To further investigate the effect of ^{90}Sr contamination and decay on the structure of C-S-H, we performed DFMD simulations at 300 K for 1.2 ps. The goal of this is to investigate if the presence of Sr and its daughter nuclei Y and Zr can lead to structural modifications of the cement paste, or if they are likely to stay in former Ca sites as assumed in Sec. III A. Given the computational cost of such calculations, we focused on a single Ca site, number 56 in our notation, which is situated in the interlayer spacing. This site is a good candidate to test our hypotheses. Since its substitution energy is average for Sr and larger than average for Y and Zr, the daughters are likely to migrate.

For the DFMD simulations, we have used a temperature control based on velocity rescaling. In this scheme, the velocities are rescaled if the average temperature and

TABLE I. Average substitution energy (eV) calculated on all the 72 substitution Ca sites and separately on the 48 intralayer sites and on the 24 interlayer sites.

	Total	Intralayer	Interlayer
Sr	0.15	0.19	0.08
Y	0.05	0.11	-0.09
Zr	2.34	2.49	2.04

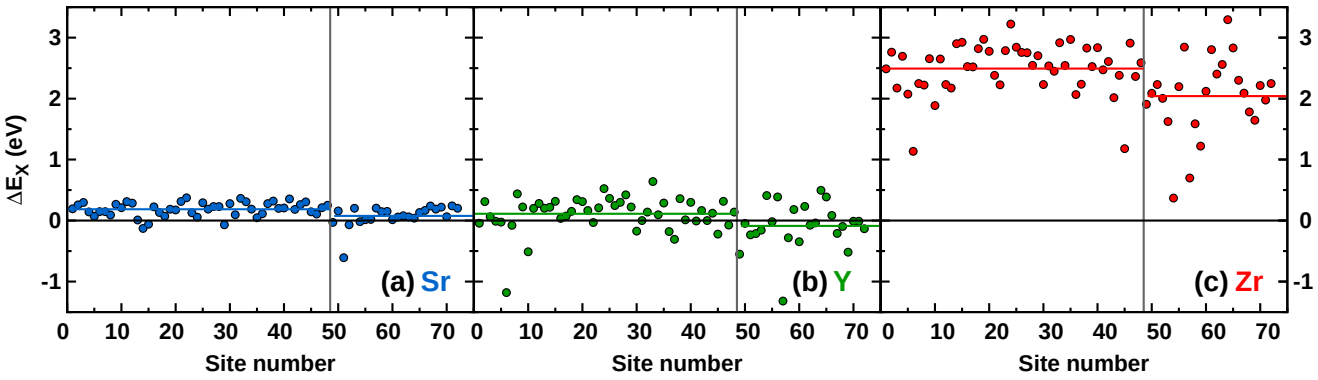

FIG. 2. (color online) Substitution energies for (a) Sr, (b) Y, and (c) Zr (circles) in the 72 Ca sites. The horizontal lines stand for the average substitution energy value, calculated separately for the intralayer and interlayer.

the target temperature of the system differ in more than a certain tolerance, which here was set to 50K.

The thermal relaxation of Sr56, Y56 and Zr56 during the simulated time range was investigated by studying the displacements of the three substitute atoms. The results are presented in Fig. 3. The displacements were found to be rather small, not exceeding 1.5 Å, as one would expect in such short simulations. Fig. 3(a) shows that Sr56 (in blue) travels a maximum distance of 0.5 Å before 0.6 ps, after which it starts moving away from its original position rather quickly before stabilizing again. Y56 does not move much away from its original position. The maximum total displacement calculated remains under 0.5 Å over the complete DFMD simulation. The displacement of Zr56 (orange) is qualitatively different from Sr56 and Y56. Not only it is larger, but it increases monotonically from the start of the simulation, thus suggesting that Zr is not stable in the interlayer Ca sites.

The distance traveled by Sr56, Y56 and Zr56 can be decomposed into the contributions along the x, y and z directions, as shown in Fig. 3(b), (c) and (d). Figure 3(b) shows that the large increase of distance starting at 0.6 ps in Sr56 is mainly due to displacements of equal amplitudes in the y and z directions, i.e. along the $[01\bar{1}]$ direction which is perpendicular to the silicate layers (see Fig. 1). The variations in the x direction are small after thermalization, and stabilize close to zero after 0.4 ps. The same is valid for Zr56 (see Fig. 3(d)), where the largest displacements are also along the $[01\bar{1}]$ direction, although in this case the displacement continues increasing over time. Fig. 3(c) shows that the total displacement calculated for Y56 is due to small oscillations of this atom around its original position in the three directions, due to thermal motion.

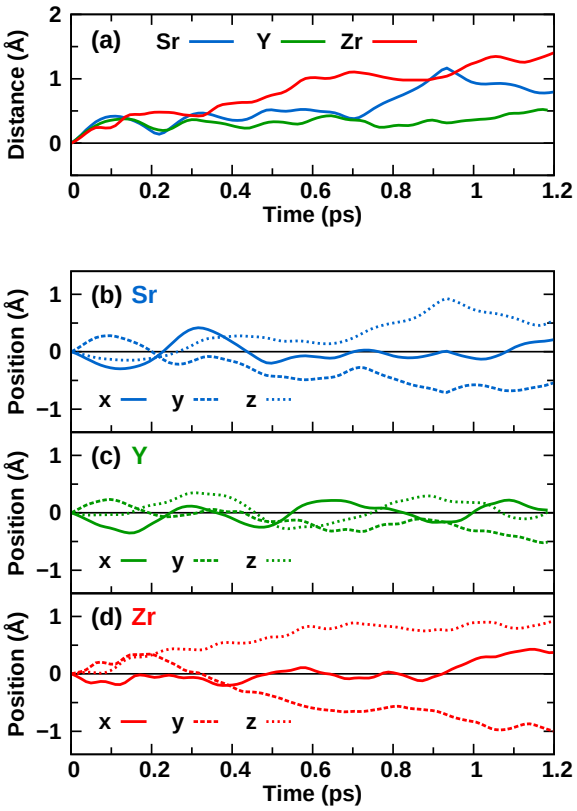

FIG. 3. (color online) (a) Distance traveled by Sr56 (blue), Y56 (green) and Zr56 (orange) as a function of time; and evolution of the position of (b) Sr56, (c) Y56 and (d) Zr56 with time at 300 K, along the x (plain lines), y (dashed lines) and z (dotted lines) direction.

The configurations reached after 1.2 ps of DFMD simulation were relaxed back to 0 K using the same convergence criterion on the total energy and forces used for the substitution energy calculations from Sec. III A. This calculation was performed in order to verify whether the ground state energies obtained after the thermal rearrangement are similar to those displayed in Fig. 2. Before the DFMD simulation, the Y-Sr energy difference was 0.37 eV and the Zr-Sr energy difference was 2.82 eV, i.e. site 56 did not exactly respect the global trend ac-

cording to which Y is slightly more stable than Sr. After the 1.2 ps DFMD simulation and quenching back to 0 K, we found that the substitution energy for site 56 reverts, now conforming to the hierarchy previously calculated: it is lowest for Y, small for Sr and large for Zr. The energy differences are now -0.05 eV for Y-Sr and 2.88 for Zr-Sr, thus validating the previous approach.

IV. DISCUSSION

A. Pair distribution

In order to investigate the physical origin of the relative stability of Sr, Y, and Zr in the cement paste, we calculated the pair distribution function (PDF) for the X-O bonds at 0 K (X = Ca, Sr, Y, Zr). We compare the PDF with the average bond lengths obtained by Shannon from an extensive compilation of crystallographic data.[38,39] The pair distributions are shown as solid black lines in Figures 3(a) to (d).

The PDF for Ca-O is shown in Fig. 3(a) along with the value of 2.40 Å tabulated by Shannon for the Ca-O bond length, which is indicated by a vertical line. The average Ca-O bond length was calculated to be 2.43 Å, in good agreement with the tabulated value. These values are reported in Table II. The Sr-O PDF is shown in Fig. 4(b). Its maximum is shifted to larger distances compared to the Ca-O pair distribution, in good agreement with the tabulated value. The corresponding Sr-O bond length, 2.56 Å, is also close to the tabulated value of 2.58 Å. The Y-O pair distribution shown in Fig. 4(c) is shifted towards lower distances compared to the Ca-O pair distribution. The bond length was found to be 2.36 Å, which is slightly larger than the tabulated bond length of 2.30 Å. The 0 K Zr-O bond length is the lowest (2.23 Å) and displays the largest discrepancy with the tabulated value of 2.12 Å. This can be correlated to the large substitution energies found for Zr in Sec. III.

The pair distributions for the intralayer and interlayer sites do not show substantial differences. To illustrate this point, we report in Table II the average bond length for these two regions. The maximum difference calculated between the intra and interlayer X-O distances is 0.02 Å for Zr, which is very small compared to differences among elements and hence does not explain the general preference for Ca substitution in the interlayer region found in Sec. III A.

In Figures 4(b) to (d) the colored lines show the pair distributions calculated for the X56-O bond at two different temperatures: 0 K (solid colored lines) and 300 K, averaged over the stable 1 ps part of the DFMD simulation (dashed colored lines).

The pair distribution for Sr56-O at 0 K (Fig. 4 (b)) is close to the average Sr-O pair distribution resulting in bond lengths that are similar (see Table II). The same applies to the pair distributions and bond lengths calculated for site 56 replaced by Y and Zr at 0 K, thus confirming that site 56 is a good candidate to represent the average properties of these atoms in C-S-H.

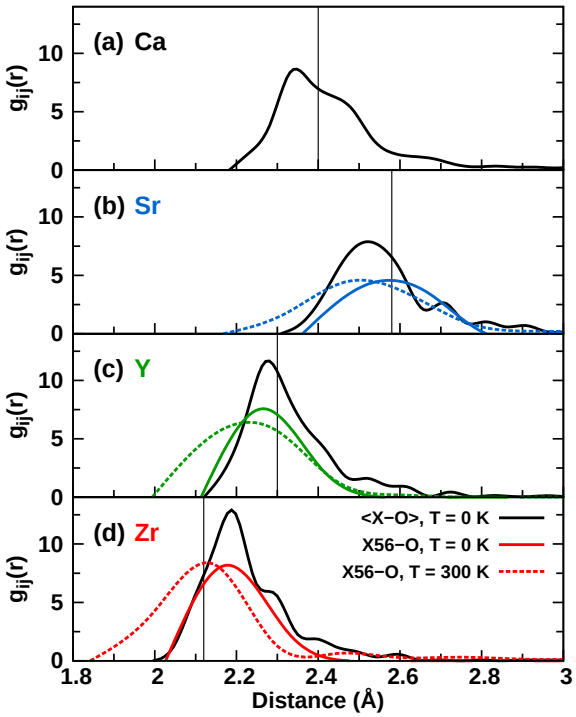

FIG. 4. (color online) Pair distribution functions for the O- (a) Ca, (b) Sr, (c) Y, and (d) Zr bonds calculated on average for all sites at 0 K (black lines), for site 56 at 0 K (solid colored lines), and for site 56 at 300 K (colored dotted line). Cubic splines have been used to smooth the pair distribution functions.

TABLE II. X-O bond lengths in the C-S-H structure. The first three columns report the average bond length calculated on all sites (Total) and separately in the intralayer (Intra) and in the interlayer (Inter) sites at 0 K. The next two columns give the X-O bond length calculated for atom X in site 56 at 0 K and at 300 K. The last column gives the corresponding values tabulated by Shannon[38,39] (Tab). All the data is given in Å.

	Average, 0 K			Site 56		
	Tot	Intra	Inter	0 K	300 K	Tab
Ca	2.43	2.43	2.43			2.40
Sr	2.56	2.56	2.57	2.58	2.53	2.58
Y	2.36	2.33	2.33	2.30	2.25	2.30
Zr	2.23	2.23	2.21	2.21	2.15	2.12

The stability of the contaminated C-S-H structure with temperature was investigated by calculating the pair distributions for the X56-O bonds on average at 300 K (dashed colored lines on Figures 4(b) to (d)), and comparing them to the pair distributions obtained at 0 K (solid colored lines). A general broadening of the PDF due to the temperature is visible on all three figures.

A slight shift to lower distances is also observed, which results in shorter average bond lengths (see Table II). This result can be due to the ability of the mobile H_2O molecules and OH^- groups from the interlayer to rearrange and form shorter bonds with the substitutional atom under the effects of temperature.

Interestingly the average bond length of Zr56-O at 300K is very close to the tabulated value of 2.12 Å. In the beginning of the DFMD simulation, Zr56 is located in the interlayer spacing, surrounded by water molecules and OH^- groups. In a second time, Zr56 migrates under the effects of temperature so that, after 0.5 ps, two of the seven nearest O atoms belong to silicate chains (SiO_4^{4-} tetrahedron). Based on the latter observation and on the isovalency of Zr with Si, it is natural to wonder whether or not it is convenient for Zr to substitute Si instead of Ca atoms in C-S-H. We investigated this possibility by substituting Zr for Si in seven (out of 44) sites. The calculated energies were all negative, varying from −2.15 eV to −0.41 eV, with an average value of −1 eV. These energies are much lower than the ones reported in Figure 2(c), and indicate that Zr will certainly interfere with the layered structure characteristic of C-S-H. This is a very interesting result that requires further investigation, e.g. via DFMD simulation over longer time scales using classical force fields to overcome the time-scale limitations imposed by the first-principles description of the interactions.

B. Analysis of the charges

The Bader charges[40] were calculated for the configurations relaxed at 0 K using the Bader Charge Analysis tool.[41] In this way we obtained 72 values of the effective charge for Ca, Sr, Y and Zr. The average effective charges for all elements are reported in Table III.

TABLE III. Average effective charge calculated on all sites (Tot) and separately in the intralayer (Intra) and in the interlayer (Inter) sites. Charge of site X56 at 0 K and 300 K. The theoretical charge for each element is given for information in the first column. All charges are expressed in the elementary charge unit e.

	Average			Site 56
	Tot	Intra	Inter	
Ca^{2+}	1.60 ± 0.04	1.59	1.61	1.60
Sr^{2+}	1.62 ± 0.04	1.61	1.63	1.66
Y^{3+}	2.22 ± 0.11	2.21	2.23	2.22
Zr^{4+}	2.28 ± 0.41	2.25	2.33	2.15

Ca and Sr are found to be isovalent, as expected, with an effective charge of approximately $1.6e$ on average. Y in Ca sites have an average charge of $2.22e$, which suggests that Y donates (on average) a large part of its valence electrons, exhibiting a charge state that is intermediate between the +2 corresponding to the substituted atom, and its own charge of +3. This results in a slightly lower substitution energy than that of Sr. Interestingly, Zr has an average charge of $2.28e$, similar to that of Y. Therefore, Zr basically fails to donate its valence electrons. This, combined with the pair distribution analysis from Sec. IV A, could explain the large substitution energies of Zr in Ca sites.

To understand the general preference for substitution in the interlayer we report in Table III the average effective charge calculated separately in the intra and interlayer regions. There is a small but systematic increase of the Bader charges in the interlayer sites with respect to the intralayer ones. This can be explained by the conspicuous presence of oxygen in the form of mobile OH^-groups in the interlayer. These can bind more easily to the substitutional ions, whereas in the intralayer the neighboring oxygens belong to the silicate chains and are thus less prone to accept electrons and stabilize the ions.

Finally, we note that the difference between inter and intralayer average effective charges increases along the radioactive decay sequence, from ^{90}Sr to ^{90}Zr. Indeed, the difference between the intralayer and interlayer average charge is the smallest for Sr and Y (around $0.02e$) and four times larger for Zr ($0.08e$). This result correlates with the substitution energy difference between the intralayer and the interlayer regions that also increases along the same decay sequence, as pointed out in Sec. III A. Similarly, the dispersion around the average value is the smallest in Sr, intermediate in Y and the largest in Zr, for both the substitution energies (see Fig. 2) and the Bader charges (see Table III).

V. SUMMARY AND CONCLUSIONS

Ab initio calculations and DFMD simulations were performed to study ^{90}Sr contamination and transmutation in C-S-H, the principal binding hydration product of cement. ^{90}Sr and its daughter radionuclide ^{90}Y were found to be stable in the cement paste, with a general preference for substituting Ca in the interlayer sites, where water enhances the possibilities for atomic bonding and charge transfer. This suggests that cement could be a good material to store the intermediate-half-life fission product ^{90}Sr, even in large concentrations. A mean field estimation gives a solubility limit of the order of 4% at room temperature, i.e., three ^{90}Sr out of 72 Ca sites. It could be relevant in the context of nuclear waste storage under accidental conditions, for example in the Fukushima case where, to the best of our knowledge, a solution to the problem of storing the highly concentrated ^{90}Sr after extraction from the emergency reactor cooling water has not been found yet.

The present work also showed that ^{90}Zr (stable daughter nucleus of ^{90}Y) is not stable in Ca sites. This suggests that ^{90}Zr is likely to migrate, either towards another more favorable region in C-S-H, or towards the outside of C-S-

H, segregating. The low substitution energies found for ^{90}Zr in Si sites indicate that ^{90}Zr could interfere with the silicate layers. Consequences of this result, such as possible modification of C-S-H mechanical properties by ^{90}Zr migration or structural damage, should be further investigated and could benefit from the use of other simulation techniques such as classical force-field molecular dynamics simulations that can reach time scales of microseconds, as opposed to the picoseconds that can be achieved using DFMD.

ACKNOWLEDGMENTS

The authors would like to acknowledge fruitful discussions with M. J. Abdolhosseini Qomi, K. J. Krakowiak, M. Bauchy, S. Yip, B. Coasne and H. Van Damme.

Part of this work was performed under the auspices of U. S. Department of Energy at Lawrence Livermore National Laboratory under contract DE-AC52-07A27344.

A. Caro work is supported by the Energy Dissipation to Defect Evolution Center (EDDE), an Energy Frontier Research Center funded by the U.S. Department of Energy, Office of Science.

* saul@cinam.univ-mrs.fr

[1] Weber, W. J.; Ewing, R. C.; Catlow, C. R. A.; de la Rubia Diaz, T. D.; Hobbs, L. W.; Kinoshita, C.; Matzke, H.; Motta, A. T.; Nastasi, M.; Salje, E. K. H. *J. Mater. Res.* **1998**, *13*, 1434.

[2] Ewing, R. C.; Weber, W. J.; linard, F. W. *Prog. Nucl. Energ.* **1995**, *29*, 63.

[3] Wigeland, R.; Bauer, T. H.; Morris, E. E. *Nucl. Technol.* **2007**, *154*.

[4] Kinoshita, N.; Sueki, K.; Sasa, K.; Kitagawa, J.-i.; Ikarashi, S.; Nishimura, T.; Wong, Y.-S.; Satou, Y.; Handa, K.; Takahashi, T.; Sato, M.; Yamagata, T. *Proc. Natl. Acad. Sci.* **2011**, *108*, 19526–19529.

[5] Chino, M.; Nakayama, H.; Nagai, H.; Terada, H.; Katata, G.; Yamazawa, H. *J. Nucl. Sci. Technol.* **2011**, *48*, 1129–1134.

[6] Kobayashi, D.; Okouchi, T.; Yamagami, M.; Shinano, T. *J. Plant Res.* **2014**, *127*, 51–56.

[7] Shibata, T.; Solo-Gabriele, H.; Hata, T. *Env. Sci. Tech.* **2012**, *46*, 3618–3624.

[8] Atkins, M.; Glasser, F. *Waste Manage.* **1992**, *12*, 105 – 131.

[9] Weber, W. *Nucl. Instrum. Meth. B* **1988**, *32*, 471 – 479.

[10] Pascucci, M. R.; Hutchison, J. L.; Hobbs, L. W. *Radiation Effects* **1983**, *74*, 219–226.

[11] Marks, N. A.; Carter, D. J.; Sassi, M.; Rohl, A. L.; Sickafus, K. E.; Uberuaga, B. P.; Stanek, C. R. *Journal of Physics: Condensed Matter* **2013**, *25*, 065504.

[12] Jiang, C.; Stanek, C.; Sickafus, K.; Uberuaga, B. *Phys. Rev. B* **2009**, *79*, 104203.

[13] Jiang, C.; Uberuaga, B. P.; Sickafus, K. E.; Nortier, F. M.; Kitten, J. J.; Marks, N. A.; Stanek, C. R. *Energy Environ. Sci.* **2010**, *3*, 130.

[14] Mobasher, N.; Bernal, S. A.; Kinoshita, H.; Sharrad, C. A.; Provis, J. L. *Journal of Materials Research* **2015**, *FirstView*, 1–9.

[15] Jantzen, C.; Glasser, F.; Lachowski, E. *J. Am. Ceram. Soc.* **1984**, *67*, 668–673.

[16] S., P.; Y., S.; K., K.; Y., F.; Y., A. *Proceedings of the Int. Conference on Ageing of Materials and Structures* **2014**,

[17] Jantzen, C. M. *J. Am. Ceram. Soc.* **1984**, *67*, 674–676.

[18] Cau-dit Coumes, C. In *Cement-Based Materials for Nuclear Waste Storage*; Bart, F., Cau-di Coumes, C., Frizon, F., Lorente, S., Eds.; Springer New York, 2013; pp 171–191.

[19] Atkins, M.; Cowie, J.; Glasser, F.; Jappy, T.; Kindness, A.; Pointer, C. *MRS Proceedings* **1989**, *176*, 117.

[20] Quilin, K.; Duerden, S.; Majumdar, A. *MRS Proceedings* **1993**, *333*.

[21] Jiang, W.; Wu, X.; Roy, D. *MRS Proceedings* **1992**, *294*.

[22] Wieland, E.; Tits, J.; Kunz, D.; Dähn, R. *Environ. Sci. Technol.* **2008**, *42*, 403–409.

[23] Tits, J.; Wieland, E.; Muller, C.; Landesman, C.; Bradbury, M. *J. Colloid. Interf. Sci.* **2006**, *300*, 78 – 87.

[24] Evans, N. *Cem. Concr. Res.* **2008**, *38*, 543–553.

[25] Youssef, M.; Pellenq, R. J.-M.; Yildiz, B. *Phys. Chem. Earth* **2014**, *70-71*, 39–44.

[26] Abdolhosseini Qomi, M.; Krakowiak, K.; Bauchy, M.; Stewart, K.; Shahsavari, R.; Jagannathan, D.; Brommer, D.; Baronnet, A.; Buehler, M.; Yip, S.; Ulm, F.-J.; Van Vliet, K.; Pellenq, R.-M. *Nat. Commun.* **2014**, *5*, 4960.

[27] Abdolhosseini Qomi, M.; Bauchy, M.; Ulm, F.-J.; Pellenq, R.-M. *J. of Chem. Phys.* **2014**, *140*, 054515.

[28] Pellenq, R. J.-M.; Kushima, A.; Shahsavari, R.; Van Vliet, K. J.; Buehler, M. J.; Yip, S.; Ulm, F.-J. *Proc. Natl. Acad. Sci.* **2009**, *106*, 16102–16107.

[29] Taylor, H. *Advanced Cement Based Materials* **1993**, *1*, 38 – 46.

[30] Bonaccorsi, E.; Merlino, S.; Kampf, A. R. *J. Am. Ceram. Soc.* **2005**, *88*, 505 – 512.

[31] Bonaccorsi, E.; Merlino, S.; Taylor, H. *Cement and Concrete Research* **2004**, *34*, 1481 – 1488.

[32] Allen, A. J.; Thomas, J. J.; Jennings, H. M. *Nat. Mater.* **2007**, *6*, 311–316.

[33] Richardson, I. *Cem. Concr. Res.* **1999**, *29*, 1131–1147.

[34] Richardson, I. G.; Groves, G. W. *J. Mater. Sci.* **1992**, *27*, 6204–6212.

[35] Groves, G. W.; Le Sueur, P. J.; Sinclair, W. *J. Am. Ceram. Soc.* **1986**, *69*, 353–356.

[36] Giannozzi, P. et al. *J. Phys.: Condens. Matter* **2009**, *21*, 395502.

[37] Perdew, J. P.; Burke, K.; Ernzerhof, M. *Phys. Rev. Lett.* **1996**, *77*, 3865–3868.

[38] Shannon, R. D.; Prewitt, C. T. *Acta Crystallogr. B* **1969**, *25*, 925–946.

[39] Shannon, R. D. *Acta Crystallogr. A* **1976**, *32*, 751–767.

[40] Bader, W. F. W. *Atoms in Molecules: A Quantum Theory*; Oxford University Press: New York, 1990.

[41] Tang, W.; Sanville, E.; Henkelman, G. *J. Phys.-Condens. Mat.* **2009**, *21*, 084204.
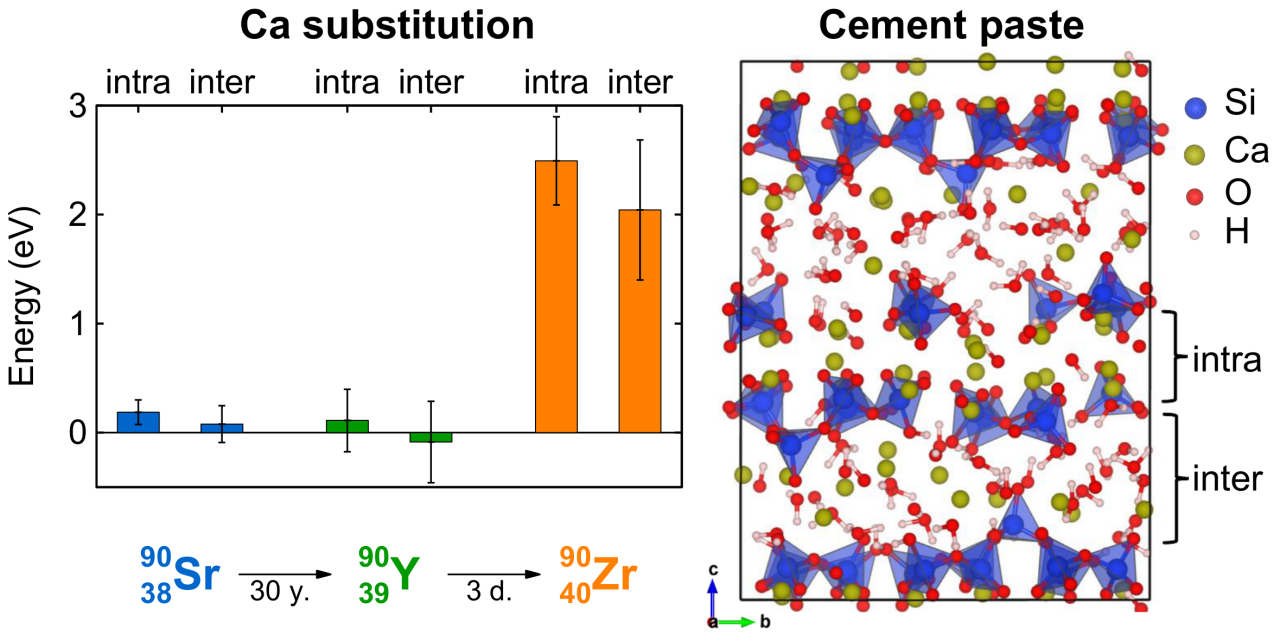
For Table of Contents Only